Experimental investigation on mechanical behavior of sandwich structures using Digital Image Correlation (DIC)

Amina Masmoudi, Abdelhak Khechai, Ahmed Bouaziz
Laboratory of Research in Civil Engineering, Mohamed Khider University of Biskra, Algeria.
amina.masmoudi@univ-biskra.dz , https://orcid.org/0009-0003-3212-7743
a.khechai@univ-biskra.dz, ahmed.bouaziz@univ-biskra.dz

Guerira Belhi
Mechanical Engineering Laboratory, University of Biskra, Algeria.
b.guerira@univ-biskra.dz

Afaf Zeroual, Yassine Adimi
Laboratory of Research in Civil Engineering, Mohamed Khider University of Biskra, Algeria.
Afaf.zeroual@univ-biskra.dz, yassine.adimi@univ-biskra.dz

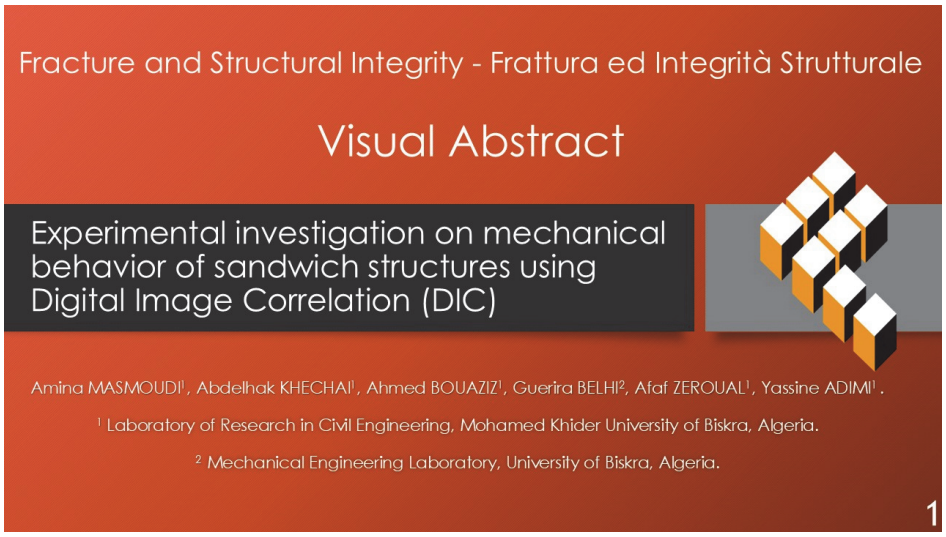

Citation: Masmoudi, A., Khechai, A., Bouaziz, A., belhi, G., Zeroual, A., Adimi, Y., Experimental investigation on mechanical behavior of sandwich structures using Digital Image Correlation (DIC), Fracture and Structural Integrity, 73 (2025) 41-58.

Received: 25.02.2025
Accepted: 10.04.2025
Published: 13.04.2025
Issue: 07.2025

KEYWORDS. Sandwich structure, PU, GFRP, Behavior, DIC.

INTRODUCTION

Sandwich structures are extensively used as structural materials across diverse industries, including civil structure and construction. This increased use is due to their remarkable strength-to-weight ratio, corrosion resistance, and durability. The design of sandwich structures, with thin, strong skins and a thick lightweight core, provides stiffness in compressive, tensile, bending, and buckling loadings [1]. The incorporation of fiber-reinforced polymers (FRP) as skins

or facesheets is commonly applied in fabricating sandwich structures owing to their high specific strength/stiffness properties and improved fatigue life, and because of the complexity of their microstructure, the damage mechanisms should be fully studied [2,3]. One of the reasons of the wide application of sandwich panels is their lightweight nature, which facilitates the transportation and assembly[1]. This low weight is typically gained from the core material. Polyurethane (PU) foam appears as the most frequently core material used thanks to their good insulation properties, having low density, good impact, and shock absorption. As highlighted by Khan et al [4], polyurethane foam (PUF) cores have become a staple in the construction industry for sandwich structures. These structures are widely used in commercial, industrial, and residential buildings, functioning as both structural walls and non-structural elements. These papers [5–7] studied the application of sandwich structures in civil engineering demonstrating their versatility to various difficulties in bridges and building constructions such as floors, roofs or walls.

Due to the complexity of sandwich structures, the requirement of studying and understanding their performance and failure characteristics have raised. Current research have illustrated that the application of fiber reinforced composite sandwich structure in construction can be efficiently and economically [8]. Experimental and numerical investigations on the mechanical behavior of sandwich structures have been discussed by several researchers. Tuwair et al. [9] investigated different core alternatives for GFRP foam-infill sandwich bridge deck panels. Three polyurethane foam core designs were tested: a high-density foam, a grid filled with low-density foam, and a special trapezoidal design with GFRP reinforcement. They assessed compressive and tensile strengths through the flatwise compressive and tensile tests. In addition, Xie et.al[10] examined the mechanical behavior of fiber-reinforced polymer sandwich structures subjected to three-point bending and double-cantilever-beam tests. They used polyurethane foam of different densities, infused with galvanized metal tooth nails as core. Results showed the improvement of both shear and compressive strength with the increase of foam density. Also Cui et al [11] studied the mechanical behavior of sandwich panel under flexural and edgewise compression loadings. The panels were made of fiber-reinforced geopolymer composite faces and PU foam core. They had found that the failure modes differed with varying thickness-to- length ratio when the sandwich panels are subjected to edgewise compression.

In order to comprehend and study the deformation and failure mechanisms of composites and sandwich structures, full field measurement is widely used. DIC is one of the methods used. DIC is a non-contact, optical measurement technique based on computer vision. Unlike the classical methods for displacement and deformation measuring such as pointwise strain gauge that only provide local strain at a selected point, DIC detects full field deformation on all over the surface of the sample[12]. Recently, numerous researchers have employed DIC to study the deformation of composite plates and sandwich structures[13,14]. Khechai et al [2] used DIC technique to obtain full-field strain of notched composite plates and found the results obtained were roughly similar to the numerical outputs determined by finite element analysis. Also, Hosseini-Toudeshky and Navaei [15] characterized the interphase elastic modulus of glass/epoxy composites using DIC and FEM.

The failure mechanisms of sandwich structures are determined by several factors: loading conditions, structure geometry, mechanical properties of the skin and core, and the interface between them. The use of sandwich structures exposes them to flat and edgewise compressive loads, resulting in complex failure modes [11]. Some of those modes are skin wrinkling, Euler macro buckling and macro shear buckling when the structure is under edgewise compression load, and core crushing and/ or densification when the structure is under flatwise compression load. Thus, it is required to monitor and measure the failure evolution to understand sandwich failure modes under those loadings.

The objective of this study is to investigate the mechanical response of sandwich structures. These structures consist of GFRP skins enclosing a core of PU. The paper is divided into two main parts. The first part is to investigate the mechanical and morphological characterization of GFRP skin where tensile and compression tests were conducted, while the second part is focused on the mechanical characterization of sandwich structure subjected to flatwise and edgewise compression loadings. The compression tests are performed on the sandwich panels, following ASTM C365 for flatwise and ASTM C364 for edgewise loading standards. Various sandwich structure lengths are tested under edgewise compression to understand the effect of using different geometries. During all the tests full -field displacement and full-field deformation were obtained using DIC 2D-Ncorr.

MATERIALS AND METHOD

Materials

The sandwich structure studied in this work is composed of GFRP skins and PU foam as core. The GFRP skins are made by hand lay-up technique on a 50x50 cm^2 plate of glass after applying mold release on it. The materials used for the skins are Polipol 353 unsaturated polyester resin as the matrix with a density of 1.121 g/cm^3 and chopped

strand mat glass fiber; four layers of mat, outer layer of 300 gr/m2 glass fiber and three layers of 600 gr/m2 glass fiber. Tab. 1 presents the mechanical properties of the used resin obtained through tensile test according to ASTM D638-14 [16]. The fiber weight fraction was determined by following the standard ISO 1172 [17] and it is estimated to be 36.55%. A CNC machine was used to cut the specimens from a 45x45 cm^2 plate into the desired shapes, 5 cm were removed from all the edges of the plates to avoid discrepancy in thickness (Fig.1a). The core is made of open-cell polyurethane foam with a density of 50 kg/m^3. To prevent the cutting effect, the skin and core of each specimen were cut separately and then assembled under cold pressure using epoxy resin as an adhesive (Fig.1b). All the materials used were commercially available. To create a random speckle pattern for DIC analysis, the specimens were coated with white paint and subsequently sprinkled with black paint.

Tensile properties	σ_{max} (MPa)	ε_{max} (mm/mm)	E (MPa)
Unsaturated polyester resin	29.88	0.0132	3620.02

Table 1: Mechanical properties of resin used.

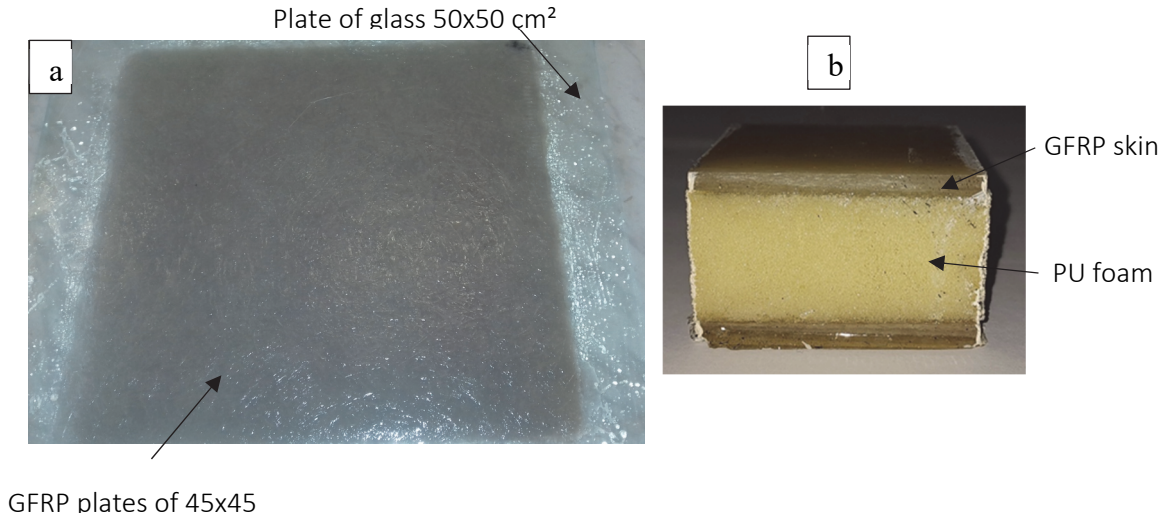

Figure 1: a) Molded GFRP plate, b) Manufactured sandwich structure.

Mechanical testing: GFRP skin

In order to investigate the mechanical performance of GFRP skin, experimental studies were carried out using an Instron 5659 Universal testing machine. The mechanical properties of GFRP skin were investigated through compressive and tensile tests, in accordance with ASTM D695-15 [18] and ASTM D638-14 [16] respectively. Fig.2 displays the specimens studied and their dimensions. Compression test methods for the skin require application of a compressive load with preventing buckling of the material [19]. Fig.3 shows the fixture for the test. Because the interface of the specimen is covered by the compressive fixture, the speckle pattern for DIC is painted on the side of the specimen.

Mechanical testing: PU core

Three specimens of 50x50x20 mm^2 were used to acquire the mechanical properties of the used foam. Flatwise compression test was carried out according to ASTM C265 [20]. The load was applied on using cylindrical loading blocks with displacement rate of crosshead of 1 mm/min.

Mechanical testing: Sandwich structure

To study the mechanical behavior of the sandwich structure, flatwise compression test was carried out in accordance with ASTM C365 [20]. The load was applied on the specimens using cylindrical loading blocks (Fig.4a and Fig.4d). The edgewise compression test was performed according to ASTM D364 [21]. The compression load was applied on the specimens using an edgewise fixture and cylindrical loading blocks (Fig.4b, Fig.4c and Fig.4e). Two different geometries of samples were studied under edgewise compression load: $w=L$ (S-60) and $w<L$ (S-200). Tab. 2 summarizes the geometrical properties of sandwich structure studied. The crosshead displacement rate for both tests was 0.5 mm/min. During compression test for

GFRP skin and both flatwise and edgewise compression tests the bottom plate was fixed and the load was applied using the top plate.

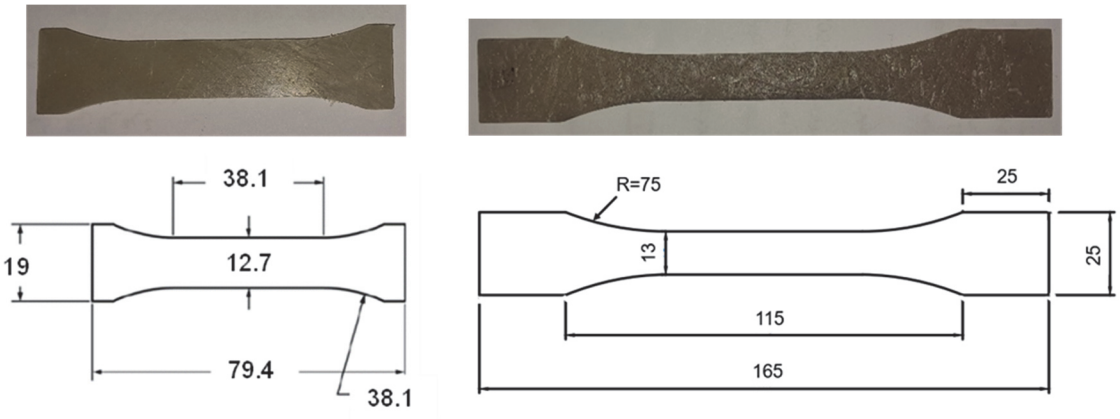

Figure 2: Geometry of GFRP skin samples used for characterization a) compressive test. b) tensile test, dimensions are in mm.

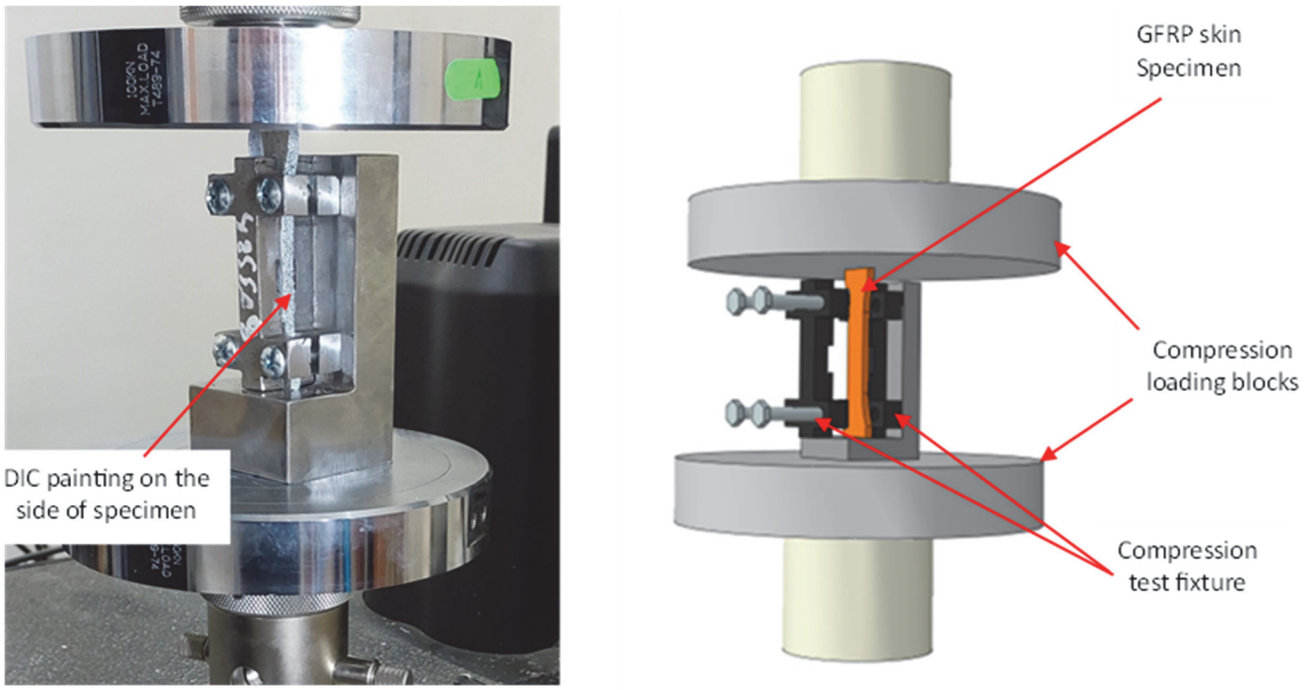

Figure 3: Compression test fixture for GFRP skin.

Scanning electron microscopy

The purpose of this study was to understand the failure mode and assess the efficiency of the fiber-matrix and skin-core bonding in samples. To achieve this, a microscopic examination was conducted using the Scanning Electron Microscopy technique at the Scientific and Technical Research Center in Physical-Chemical Analysis located in Biskra, Algeria.

Digital image correlation

DIC is an optical, full-field measurement technique that it based on computer vision. It is used in engineering and materials science to analyze the deformation and movement of objects or materials by tracking patterns or markers on their surfaces using digital image processing. DIC is widely used in areas such as structural mechanics and materials testing, to provide information on the behavior of materials and structures under different conditions. The methodology involves acquiring digital images of a surface at different stages of deformation, the analysis and comparison of these images to determine the movement of surface points, and finally the calculation of deformation maps [22]. The analysis of DIC and the subsequent

determination of strain involved the use of an open-source tool for Digital Image Correlation (2D) Ncorr [23] , which is a post-processing tool from MATLAB. To measure the displacement and strain, DIC-Ncorr code uses subsets of pixels; subset radius which refers to the size of a circular or square subset or region of interest (ROI) that is used to track and analyze the displacement or deformation of an object or material in an image sequence; subset spacing refers to the distance between the centers of adjacent subsets. The primary objective is to choose the smallest subset possible that avoids generating noisy displacement data [24]. In this study 43 pixels and 3 pixels were chosen for subset radius and subset spacing respectively. High-resolution images were recorded during the tests using camera CANON 1300D. A led source was fixed in front the machine to improve the illumination of the analyzed specimens. Fig.5 demonstrates the DIC setup used for all the tests for GFRP skin and sandwich specimens.

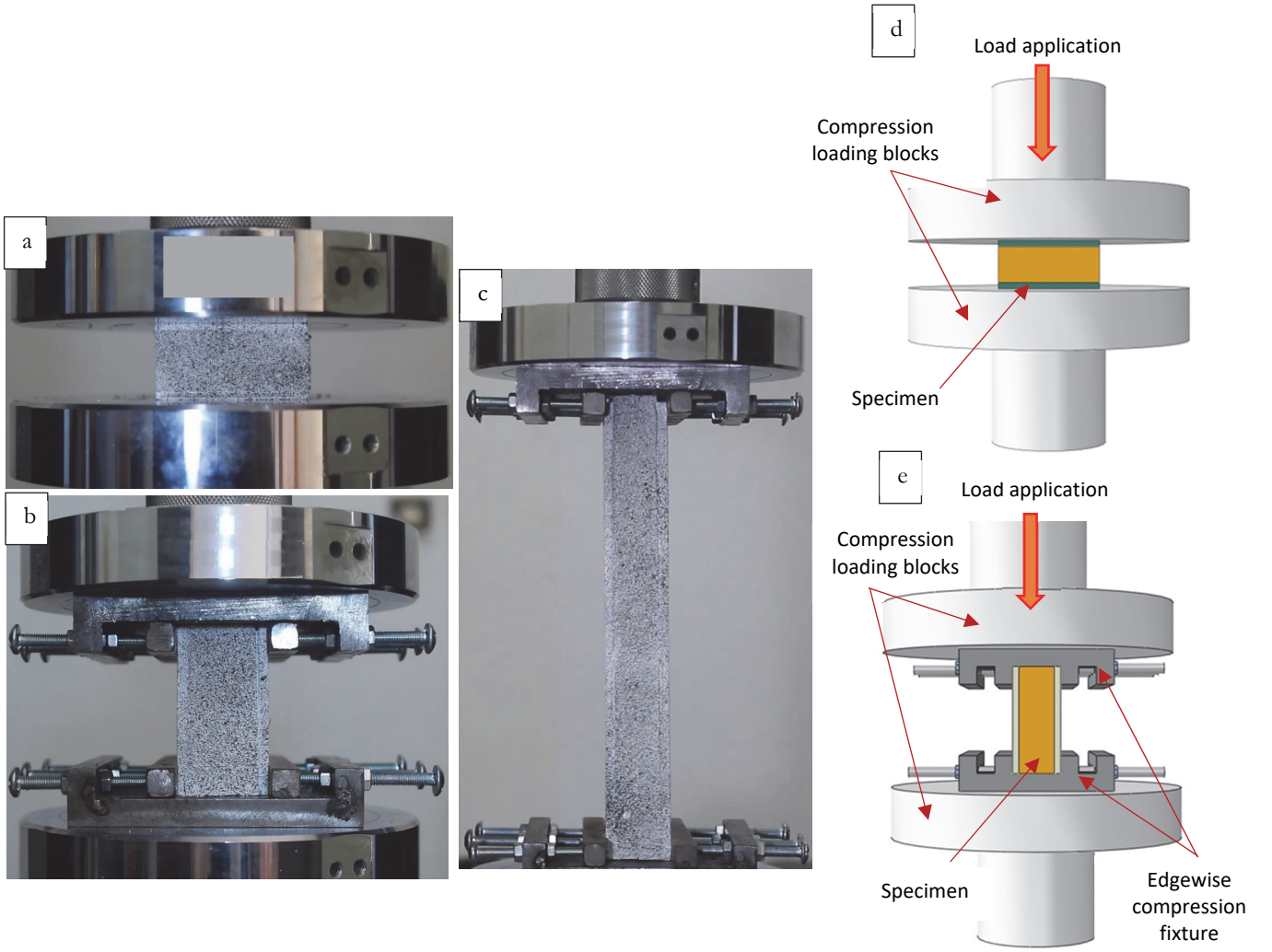

Figure 4: Sandwich compressive setup a) flatwise compression. b) edgewise compression S-60. c) edgewise compression S-200. d) Flatwise compression setup. e) Edgewise compression setup.

Dimensions	Flatwise compression test	Edgewise compression test	
		S-60	S-200
w: width (mm)	50	60	60
L: length (mm)	50	60	200
t_t: Total thickness (mm)	28.62±2.3	29±1.12	27.83±3
t_c: Core thickness (mm)	21.3±2.1	21.8±1.08	20.51±3
t_s: Skin thickness (mm)	3.67±0.35	3.8±0.15	3.62±0.15

Table 2: Geometrical properties of sandwich structure.

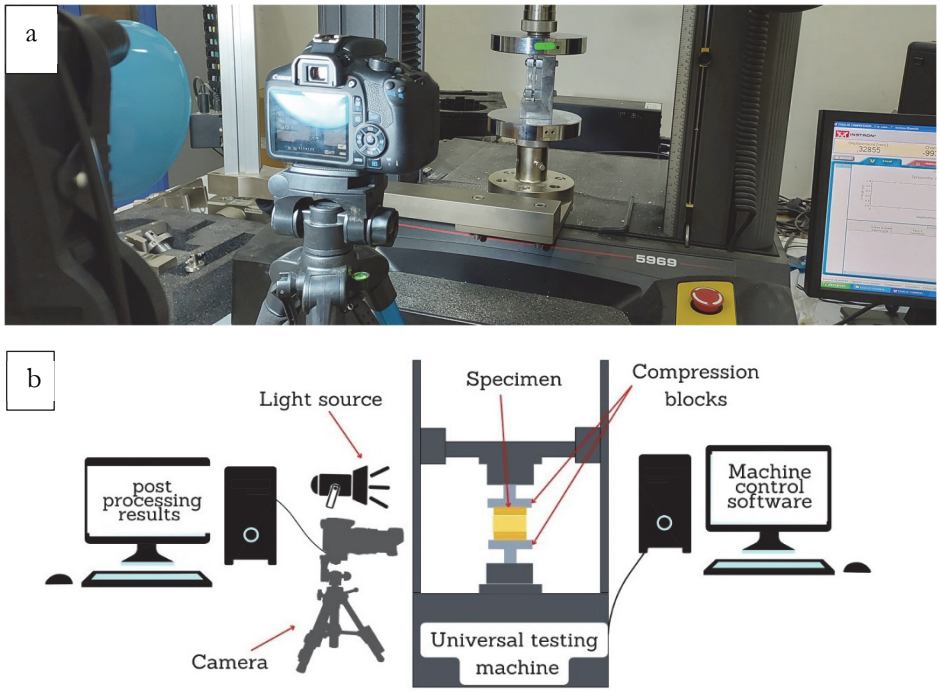

Figure 5: Experimental setup for DIC analysis adopted, a) GFRP skin compression test, b) Flatwise compression for sandwich.

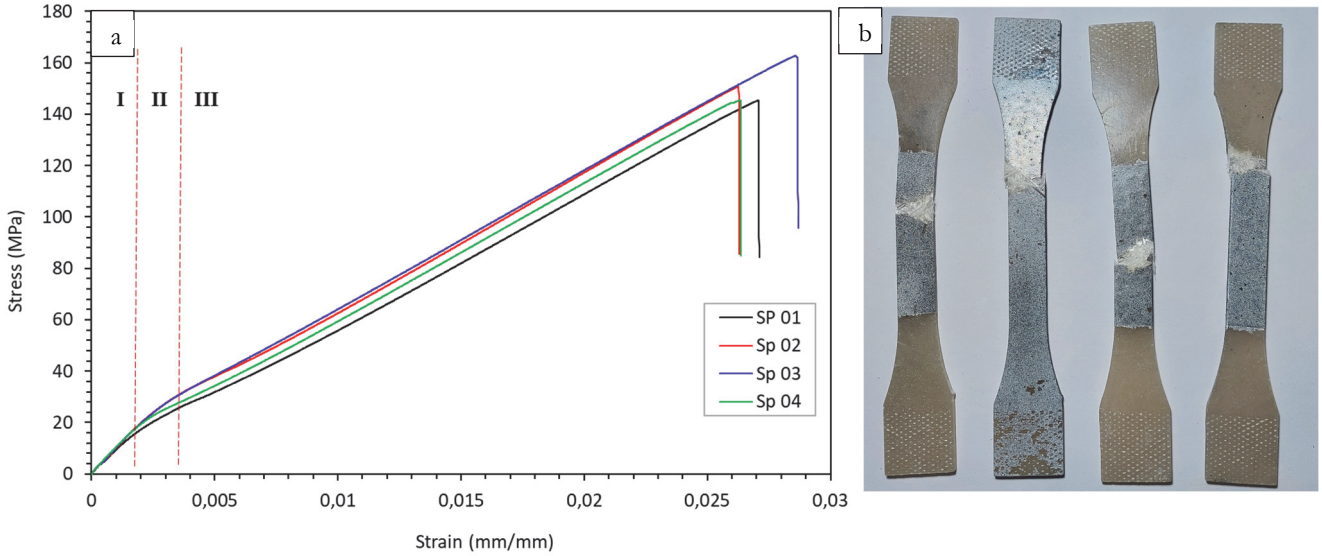

Figure 6: a) Stress-strain curves for tensile test of GFRP skin. b) Specimens after tensile test.

RESULTS AND DISCUSSION

Tensile test for GFRP skin

Fig.6a shows the stress-strain curves from the tensile test for GFRP skin. It demonstrates that the curves behave identically and approximately overlay one another, which confirms the repeatability and reliability of the GFRP skin behavior under tensile load. It is observed that this behavior is divided into three parts as demonstrated. Firstly, the behavior is mainly linear up to the point where the elastic stress is about 12.57 % of the ultimate tensile stress. Then the curves lose their linearity and the damage starts, it is defined by the elastic modulus. At the end of the elastic part, the curves exhibit a bend that could be related to prior fiber damage caused by fragile bonding between fiber and matrix. The final

phase is when tensile stress increases nonlinearly with longitudinal strain until final damage occurs. As illustrated in Fig.6b, the failure positions of the specimens after testing, were almost close to the center. Fig.7 demonstrates SEM image of fractured zone from the specimen under tensile test. One can see an irregular distribution of glass fibers, a debonding of fiber-matrix, fiber breaking and pull out. The maps in Fig.8 represent the in-plane strain fields of the GFRP skin under tensile loading for Sp 03. The DIC images were taken just before final failure. The chromatic map displays the maximal value of strain ε_y in red 0.03, which confirming the experimental results with high accuracy. The concentration of longitudinal strain indicates the location of the fracture in the specimen. The results obtained from the tensile test are summarized in Tab. 3. All samples have approximately the same strength, and the average value is 151.12 MPa with corresponding strain of 2.7%.

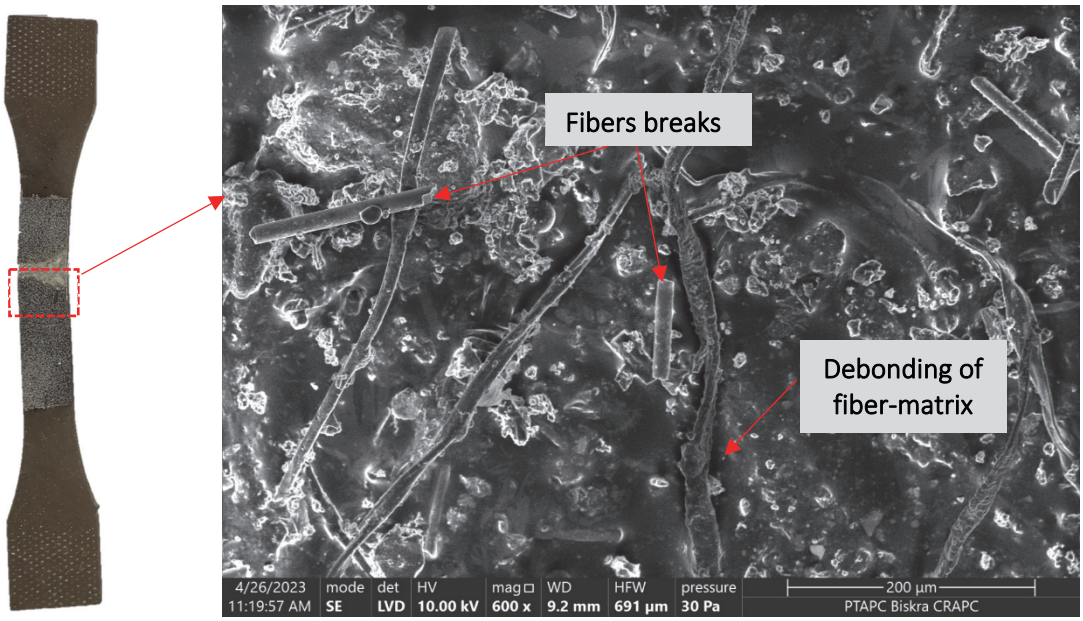

Figure 7: SEM of fracture surface of GFRP skin under tensile failure.

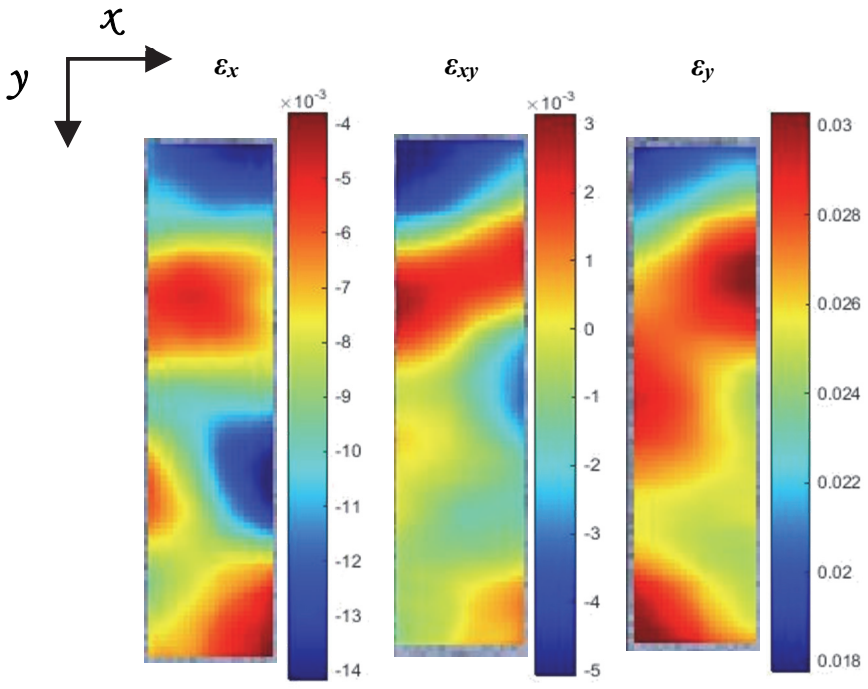

Figure 8: DIC engineering strain fields for tensile test of GFRP skin.

	Pmax (N)	Displacement (mm)	Elastic stress (MPa)	Corresponding strain (mm/mm)	Ultimate tensile stress (MPa)	Tensile strain (mm/mm)	Young's Modulus (MPa)
Sp 01	7331.99	4.47	15.54	0.0017	145.36	0.027	9656.84
Sp 02	7645.72	4.34	20.04	0.002	150.80	0.026	9899.19
Sp 03	8172.43	4.73	22.39	0.0023	162.86	0.029	9806.83
Sp 04	7430.43	4.35	18.07	0.0018	145.44	0.026	9406.89
Average	7645.14	4.47	19.01	0.0019	151.12	0.027	9692.44
SD	8.23	0.18	2.91	2.65E-04	8.23	1.0E-03	214.97

Table 3: Mechanical parameters obtained through tensile test of GFRP skin.

Compression test for GFRP skin

Fig.9a presents the stress-strain curves from the compressive test for GFRP skin. Similar to the tensile test, it is illustrated that the curves exhibit an identical behavior, which also approves the consistency of the GFRP skin behavior under compressive loading. Three distinct phases are noted. Initially, the behavior remains predominantly linear, reaching a point where the curves deviate from linearity and damage initiates; this phase is primarily characterized by the elastic modulus. Elastic stress is estimated by 2.17% of the ultimate compressive stress. At the end of the elastic phase, the curves exhibit a noticeable bend, possibly due to prior fiber damage resulting from weak bonding between the fibers and the matrix. The final phase involves a nonlinear increase in compressive stress with longitudinal strain until eventual failure or damage is observed. As it is shown in Fig.9b and Fig.10, the failure modes that occur in the specimens are localized at the center. It was evident that the observed failure involved a combination of longitudinal splitting, interlaminar cracking, fiber breakage, and the formation of kink bands, specifically manifested as fiber micro-buckling. Kim et al. had detected a comparable failure mode of GFRP composites subjected to compression [25]. Fig.11a illustrates the region of interest studied in DIC and Fig.11b presents full-field strain maps of Sp 03. The DIC images were captured just before final failure. The chromatic maps display the highest absolute values of strain ε_y 0.031 at the top, where the load is applied. On the other hand, it can be seen that the values obtained through DIC are similar to the those obtained experimentally (see Tab. 4). The maximum values of ε_x appeared in the middle of the specimen is 0.02, demonstrating the region of the local buckling happened to the sample. The results obtained from the compressive tests are listed in Tab. 4. The samples have an average strength of 226.70 MPa and 3.4 % strain.

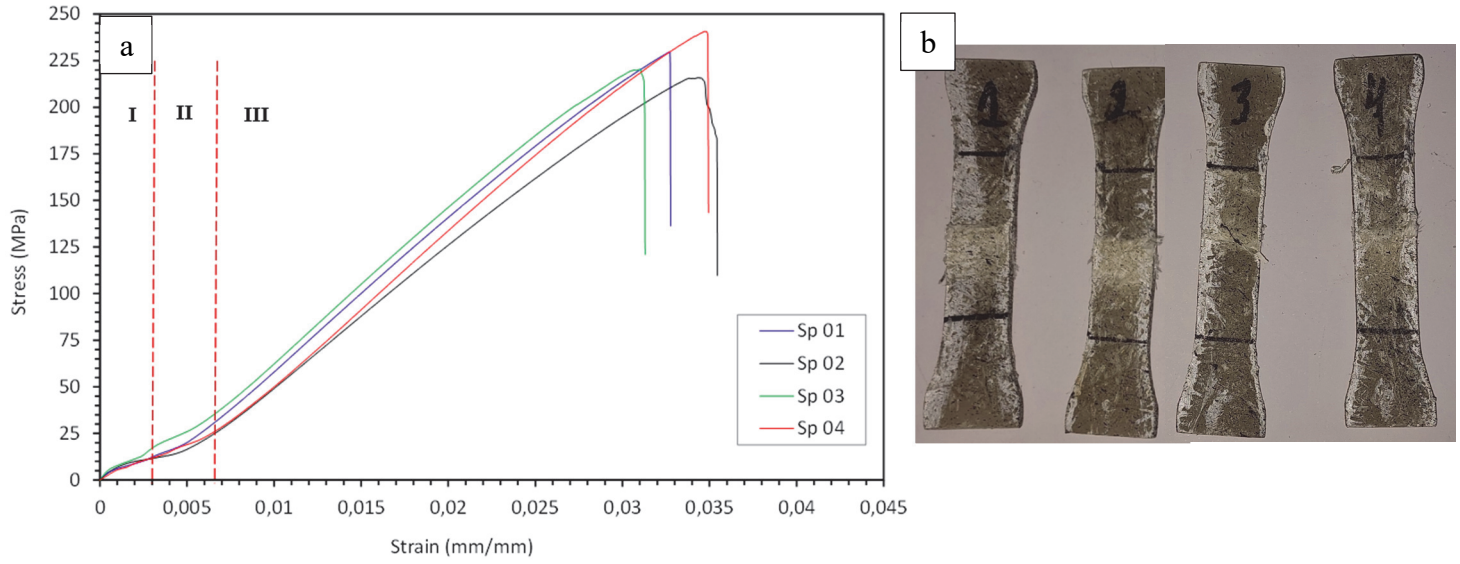

Figure 9: a) Stress-strain curves for compression test of GFRP skin. b) Specimens after compression test.

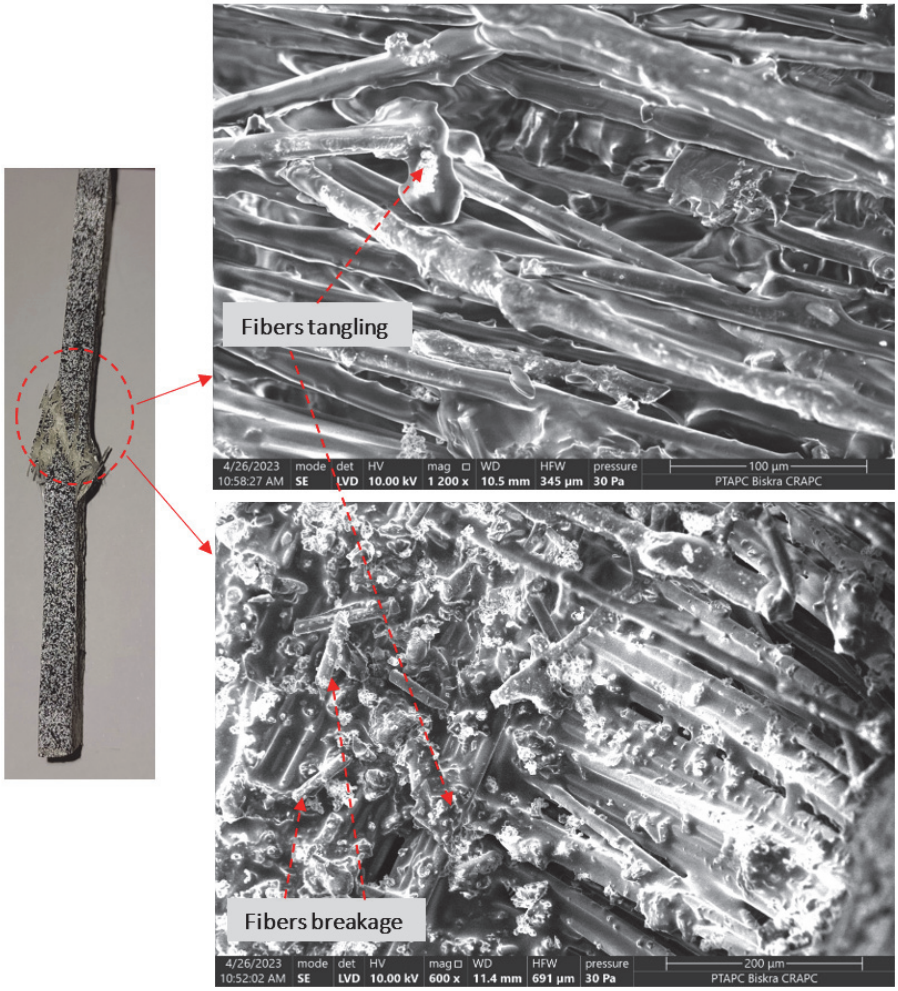

Figure 10: SEM of fracture surface of GFRP skin under compressive failure.

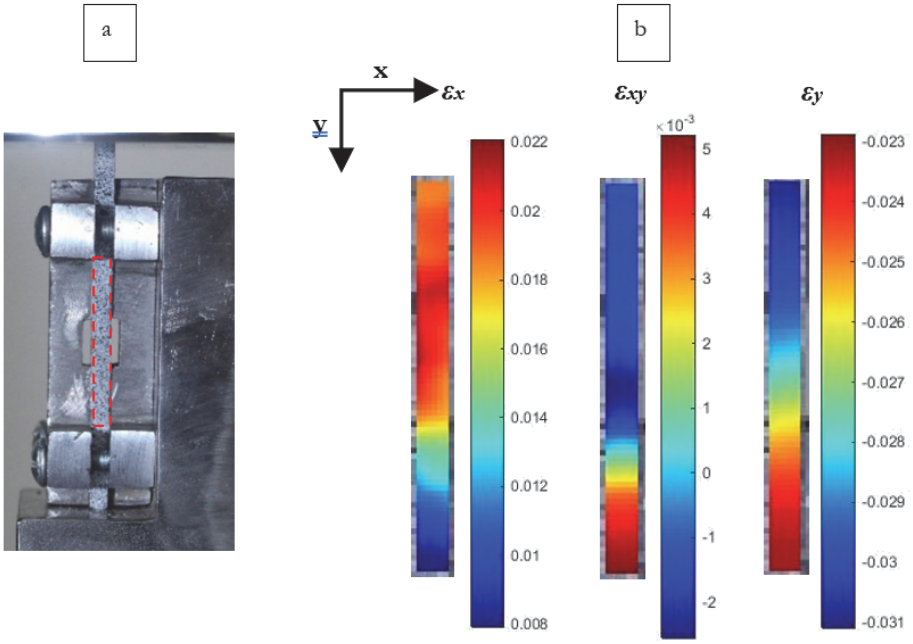

Figure 11: a) Region of interest studied in DIC, b) DIC engineering strain fields for compression test of GFRP skin.

	Pmax (N)	Displacement (mm)	Elastic stress (MPa)	Corresponding strain (mm/mm)	Ultimate compressive stress (MPa)	Compressive strain (mm/mm)	Young's Modulus (MPa)
Sp 01	12575.44	2.60	4.22	5.17E-04	229.74	0.032	9524.71
Sp 02	11680.25	2.82	5.67	7.75E-04	215.89	0.035	8643.35
Sp 03	11562.19	2.49	4.89	4.32E-04	220.44	0.031	9285.39
Sp 04	13055.18	2.77	5.53	1.03E-03	240.74	0.035	9701.55
Average	12218.27	2.67	5.08	6.88E-04	226.70	0.034	9288.75
SD	718.31	0.15	0.66	2.69E-04	10.99	1.9 E-03	462.83

Table 4: Mechanical parameters obtained through compressive test of GFRP skin.

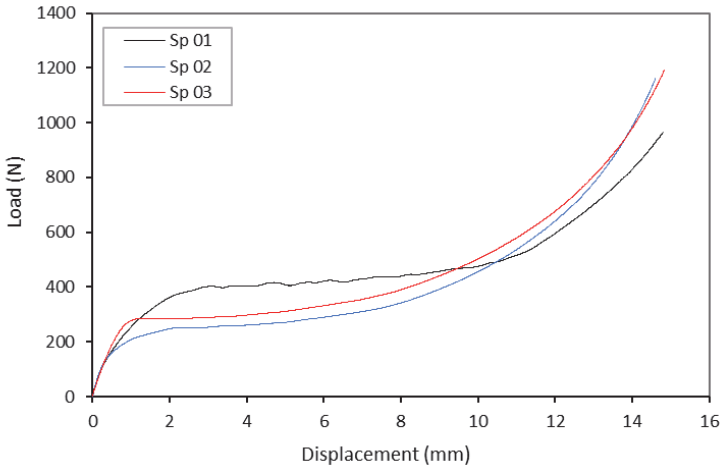

Figure 12: Compressive Load-Displacement curve for PU foam.

Properties	PU foam
Compressive stress (MPa)	0.44
Compressive strain (mm/mm)	0.74
Elastic stress (MPa)	0.1
Corresponding strain (mm/mm)	0.4
Compressive Modulus (MPa)	4.19
Shear modulus (MPa)	1.49
Poisson ratio	0.40

Table 5: Mechanical properties of PU foam.

Flatwise compression test

The results of the flatwise compression of PU foam are summarized in Fig.12 and Tab. 5. Load-Displacement curves of the studied sandwich under flatwise compression are shown in Fig.13. As it is marked, the zoomed-in region of the curves exhibits a similar behavior to polyurethane foam under compression test (Fig.12), which can be explained by that the core is the first part of sandwich to experience damage. It is noticed that the curves behave in a comparable performance; an elastic region (OA), followed by a plateau phase where the specimen starts to condense (AB), then a densification phase was noted where a rapid increasing of load with small displacement (BC). Fig.14 depicts the final failure of the specimens. Fig.15 illustrates the SEM micrograph of flatwise compression samples. The samples were cross-sectioned to obtain the SEM images Fig.15a. It is noted that no debonding between skin and core induced by testing is recorded in Fig.15b. This can be attributed to the efficient stress transfer facilitated by the strong interfacial adhesion between the GFRP skin and the PU foam core under flatwise compression. This loading mode promotes foam densification, which limits interfacial failure

and enhances the structural response. The presence of epoxy resin at the interface further improves mechanical integrity due to its high compressive strength and stiffness, enabling effective load distribution between the skin and the core. Furthermore, significant compression of the PU foam led to extensive cell collapse, making most of the foam cells no longer distinguishable. It is worth noting that the localized gaps observed at the skin–core interface are not indicative of debonding initiated during testing, but rather result from the inherent surface porosity of the foam structure and minor surface imperfections of the skin. The zoomed-in part of the sample in Fig.15c exposes microcrack in the skin parallel to the loading fixture. This microcrack may have formed as a result of continuous micro-voids. DIC results of SP 02 are shown in Fig.16. The images were taken just before losing correlation, and the map faded caused by foam compression (point F in Fig.13).

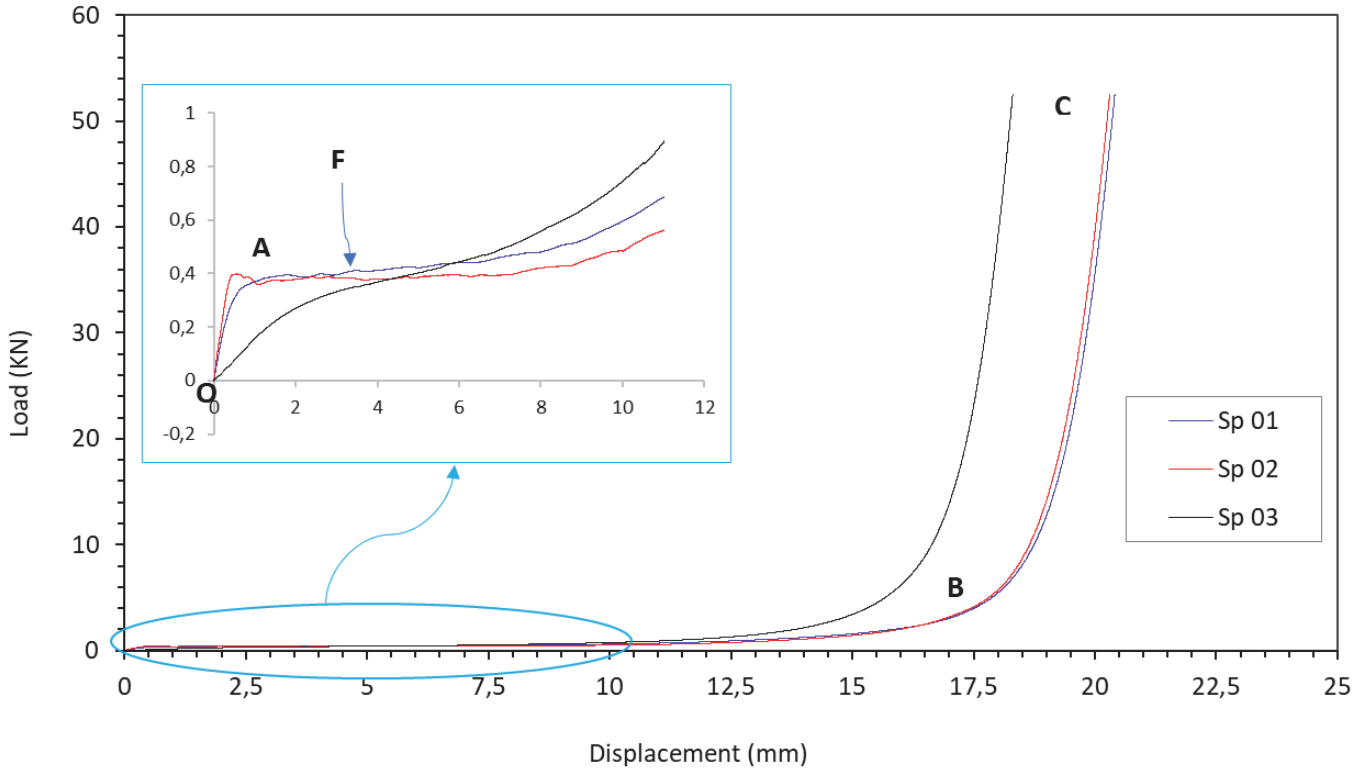

Figure 13: Flatwise compression Load-Displacement curves of sandwich structure.

It is notable that the maximum displacement along the load direction (V) is corresponding to the top plate where the load is applied, colored in red, and it gradually decreases to zero towards the bottom fixed plate. However, the displacement traverse to the loading (U) indicates the expansion of the foam on both sides in opposite directions and tends to zero in the rest of points. Furthermore, the concentration longitudinal strain $\boldsymbol{\varepsilon_y}$ in blue signifies the densification of the PU foam. The results obtained from the test are listed in Tab. 6. The average ultimate flatwise compression strength and compressive strain are 20.99 MPa and 0.69 respectively. The total displacement of the specimens attains about 70% of its initial thickness. According to ASTM C-365M the ultimate flatwise compression strength was calculated using Eqn. (1)

$$\sigma_{fc} = \frac{P_{max}}{A} \tag{1}$$

where σ_{fc} is the ultimate flatwise compressive strength (MPa). P_{max} is the ultimate force prior to failure (N) and A is the area of the of the surface of facing subjected to compressive load (mm^2).

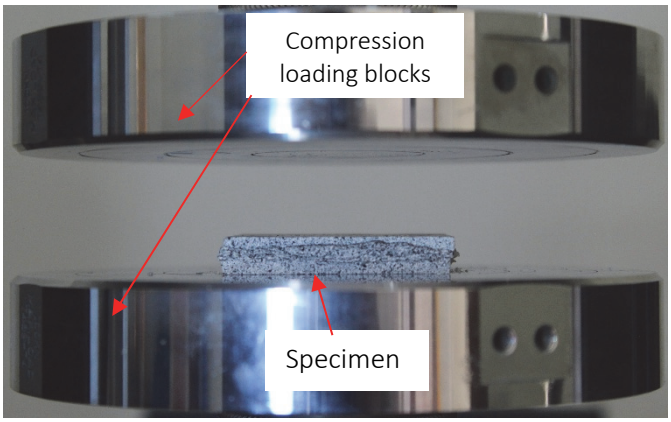

Figure 14: Specimen after Flatwise compression.

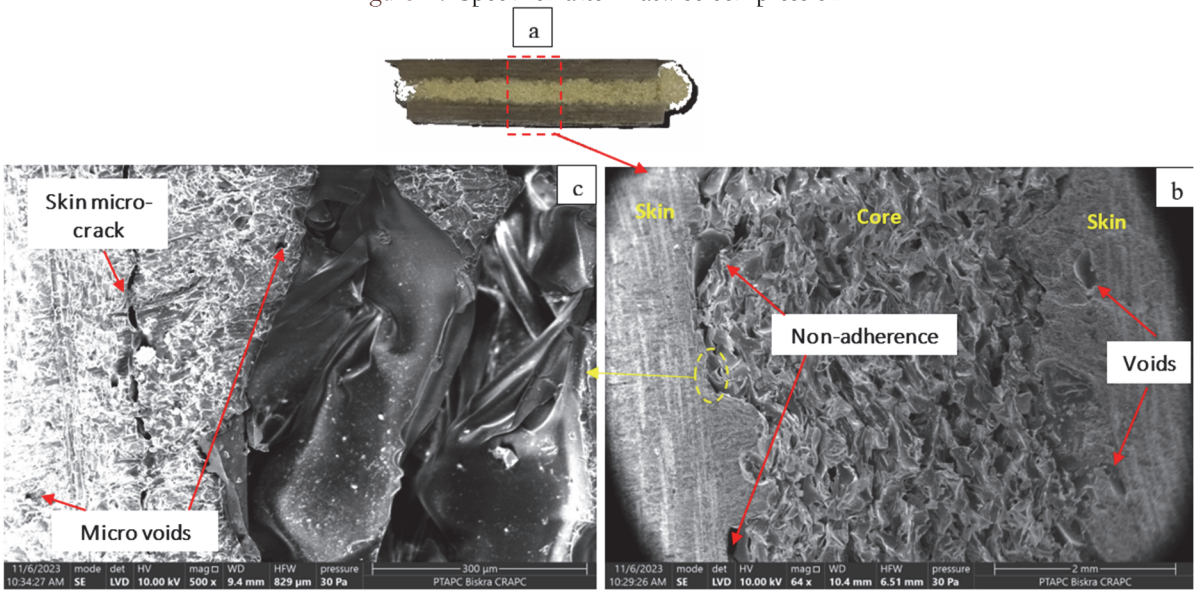

Figure 15: SEM micrographs for flatwise compression sample.

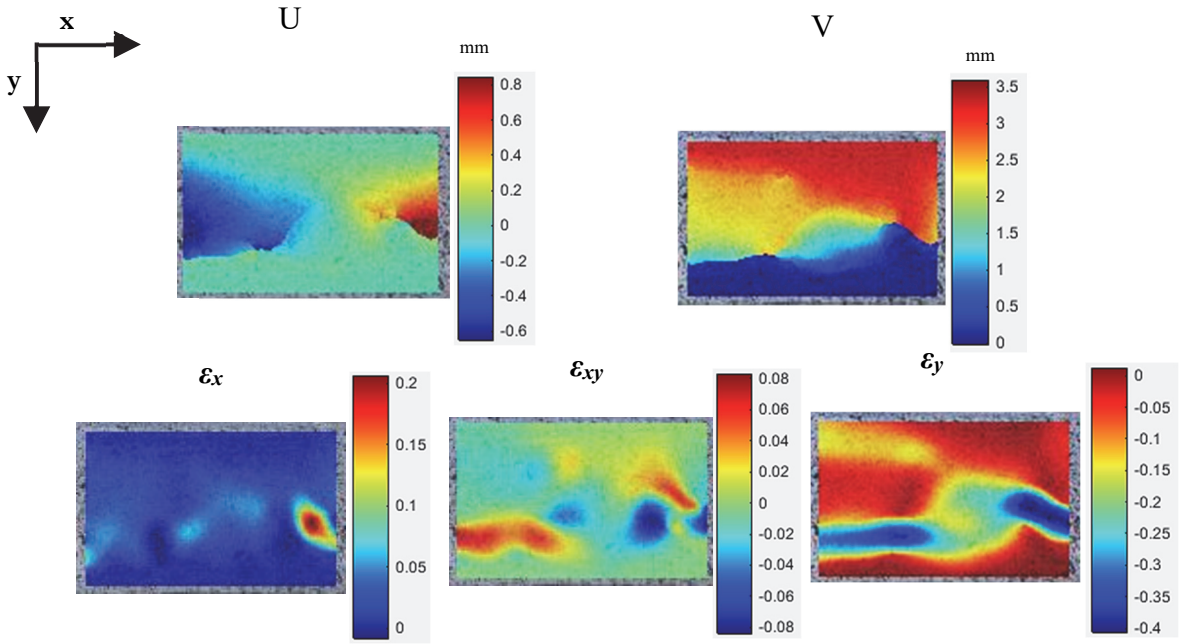

Figure 16: DIC engineering displacement and strain fields for flatwise compression test of sandwich structure.

	Pmax (kN)	Displacement (mm)	Ultimate flatwise compressive stress (MPa)	Compressive strain (mm/mm)
Sp 01	52.49	20.41	20.997	0.68
Sp 02	52.43	18.31	20.993	0.70
Sp 03	52.47	20.30	20.990	0.68
Average	52.48	19.67	20.99	0.69
SD	9.00E-03	1.18	3.50E-03	0.011

Table 6: Mechanical parameters obtained through flatwise compressive test of sandwich structures.

Edgewise compression test

Fig.17a shows the failure modes of sandwich structures under edgewise compression loading for S-60. It is observable that Sp 03 behaved differently from the other specimens, this variability is a known characteristic of compression tests for sandwich structures, as slight differences in specimen alignment, material properties, or initial defects can significantly impact the failure mode and load response. An abrupt failure caused by skin buckling, succeeded by skin-core debonding on both sides for Sp 03 with a shear sliding damage of the skin on the left side. The other three specimens experienced the same behavior until final failure; localized buckling in the mid-section of the specimens followed by skin cracking on both sides and progressed throughout the width of the specimen and a small skin-core debonding on one side. Fig.17b depicts the load-displacement curves obtained from the test for S-60. The curve for Sp 03 demonstrates a decent linearity to ultimate load then the load decreased gradually to total failure. Meanwhile, the curves of the other three specimens exhibited a similar pattern and performed an initial phase of linear increase of the applied load, followed by a non-linear phase until the ultimate load is reached, then the load decreased gradually to final failure. The average ultimate load for those three is about 37.86 KN, which is roughly twice compared of Sp 03. Fig.18a illustrates the collapse modes of S-200, where a significant difference in failures mechanisms is noticed. For S-200, different behavior was detected, the specimens collapsed in the global buckling mode or as it known Euler buckling. A densification of the foam was observed during the test for both S-60 and S-200. Fig.18b represents the load-displacement curves obtained from the test for S-200. The curves exhibit a small linear pattern succeeded by a non-linear phase until the ultimate load reached its maximum. Followed by softening phase of post-buckling. The divergence in failure modes of S-60 and S-200 samples under edgewise compression load signifies that the lengths of samples have a crucial impact. When the length is higher than the width, Euler buckling becomes the dominant failure mode, and the load capacity of the samples decreases. The ultimate load decreased from 39.76 kN to 5.1 kN with the of the length of specimens increased. DIC engineering displacement and strain fields for edgewise compression test for Sp 02 for both S-60 and S-200 are shown in Fig.19. Point A in Fig.17a and 18a indicates where the images were taken, before the correlation is lost. The collapse modes of the specimens during this test are further clarified by the displacement along the horizontal direction U. The displacement U of S-60 is small compared to S-200. The maximum displacement for S-60 is 3.5 mm and it is concentrated in the region, where it first buckled and damaged. While the maximum displacement for S-200 is 14 mm in the middle part of the sample, with the top and bottom ends have minor displacement. Summarized results are listed in Tab. 7, for S-60 the average values of the test were calculated without including Sp 03. According to ASTM C-364M the ultimate flatwise compression strength was calculated using the Eqn. (2)

$$\sigma_{EC} = \frac{P_{max}}{2.w.t_s} \tag{2}$$

where σ_{EC} the ultimate edgewise compressive strength (MPa). Pmax is the ultimate force prior to failure (N), w width of specimen (mm) and t_s thickness of a single face sheet (mm).

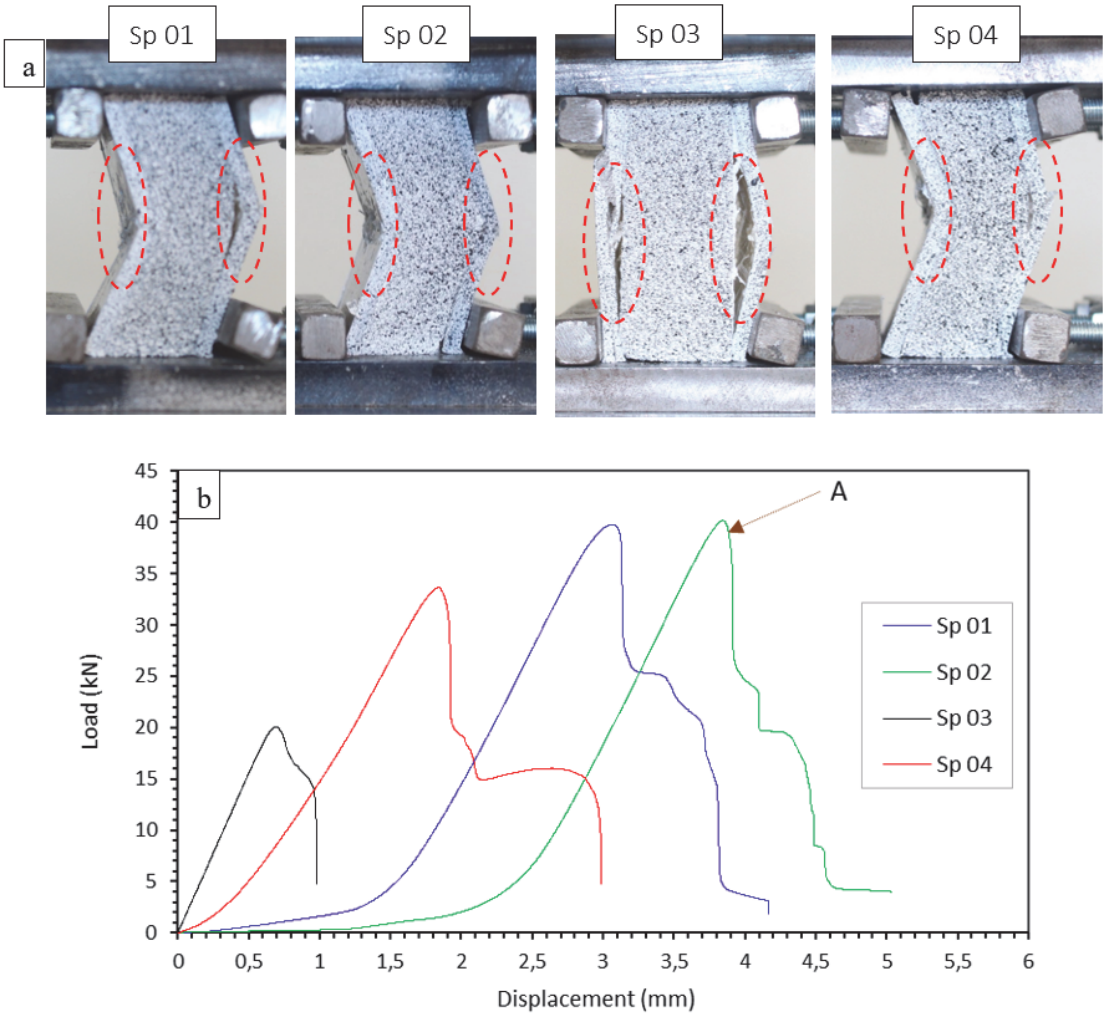

Figure 17: a) Specimens after edgewise compression test for S-60. b) Edgewise compression load-displacement curves for S-60.

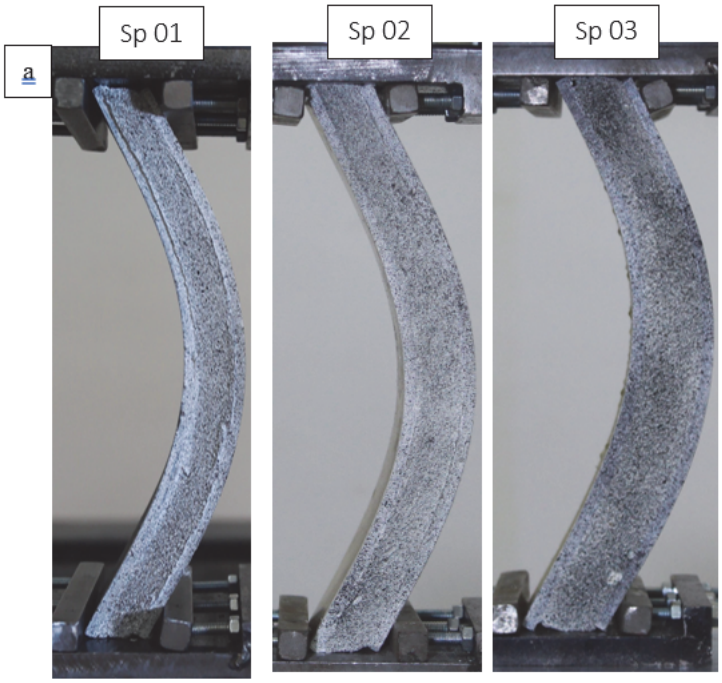

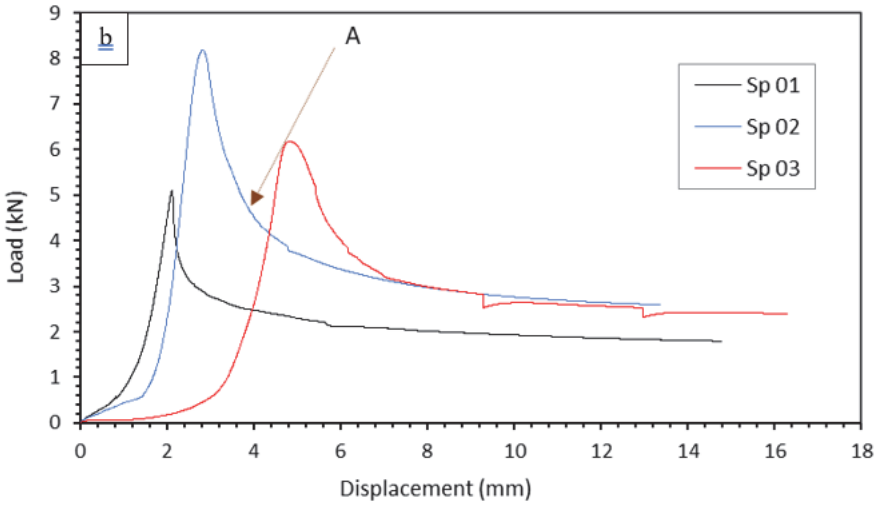

Figure 18: a) Specimens after edgewise compression test for S-200. b) Edgewise compression load-displacement curves for S-200.

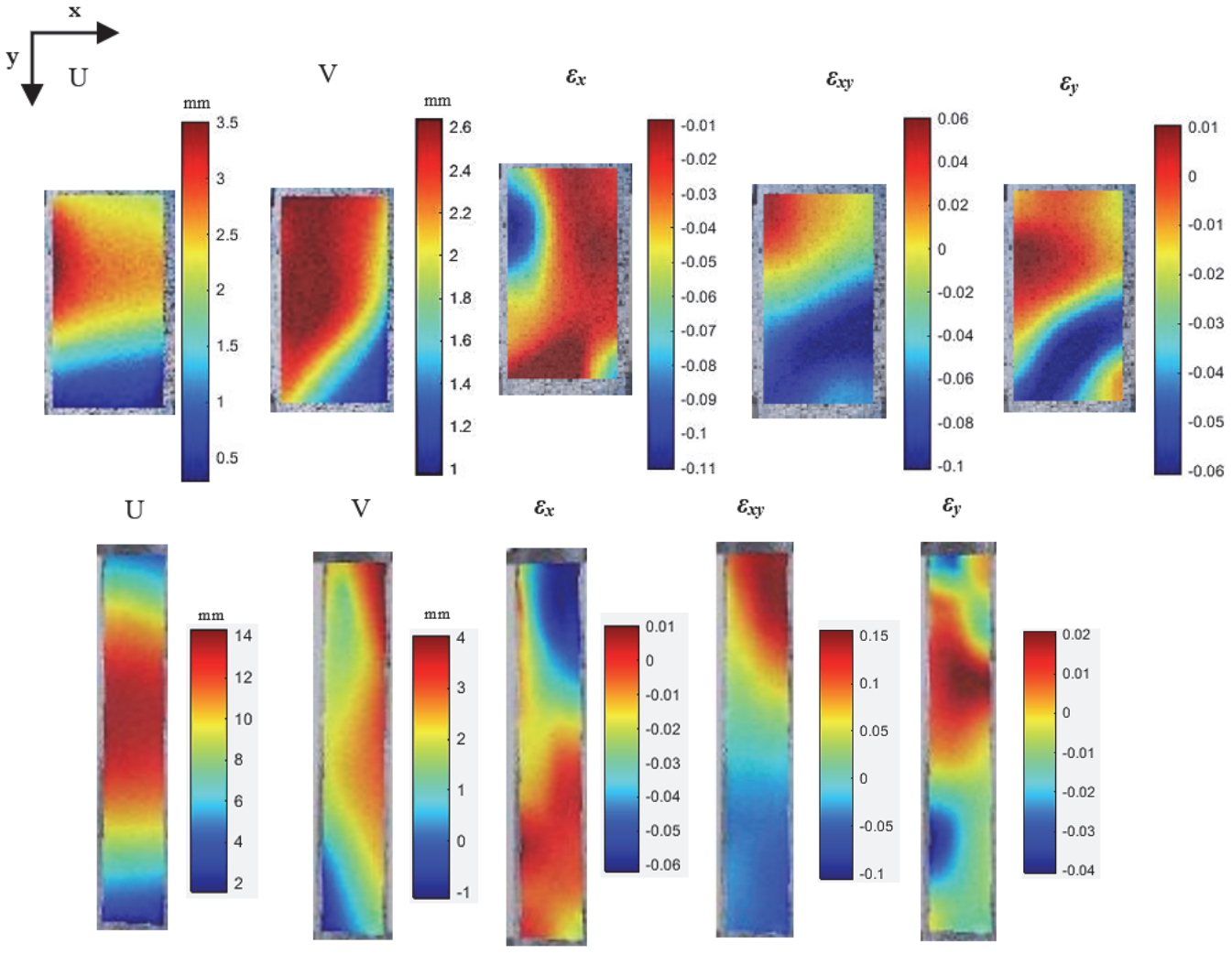

Figure 19: DIC engineering displacement and strain fields for edgewise compression for sandwich; upper row S-60, lower row S-200.

		Pmax (kN)	Displacement (mm)	Ultimate edgewise compressive stress (MPa)	Compressive strain (mm/mm)
S-60	Sp 01	39.77	4.16	87.21	0.069
	Sp 02	40.16	5.04	95.63	0.084
	Sp 04	33.65	2.99	73.79	0.049
	Average	37.86	4.06	85.54	6,73E-02
	SD	3.65	1.03	11.01	1,76E-02
	Sp 03	20.08	0.98	44.87	0.016
S-200	Sp 01	5.10	14.78	11.34	0.074
	Sp 02	8.18	13.38	17.93	0.067
	Sp 03	6.18	16.30	14.11	0.082
	Average	6.49	14.82	14.46	0.074
	SD	1.56	1.46	3.31	7.00E-03

Table 7: Mechanical parameters obtained through edgewise compressive test of sandwich for S-60 and S-200.

CONCLUSION

The behavior of sandwich structure subjected to flatwise and edgewise compression was investigated. Digital image correlation was used to study full fields measurements. Glass Fiber Reinforcement Polymer composites were used as skin and PU foam as core. Tensile and compression tests for GFRP skins were conducted to obtain mechanical characteristics. Samples of 50x50 mm² of sandwich structure were studied under flatwise compression loads. For the edgewise compression test two different geometries of sandwich structures were tested 60x60 mm² and 60x200 mm². All the tests were performed according to ASTM standards. The results obtained can be summarized as follow:

- The use of DIC throughout all tests demonstrated strong agreement with the results obtained from mechanical testing, confirming the accuracy and reliability of DIC measurements.
- GFRP skins illustrated an ultimate tensile strength of 151.12 MPa and a compressive strength of 226.70MPa. the microscopic study shows different mechanisms; debonding of fiber-resin, fiber breaking and pull out for tensile samples and combination of longitudinal splitting, interlaminar cracking, fiber breakage for compressive samples.
- Sandwich structures encountered condensation and densification of PU foam with micro cracks in GFRP skin under flatwise compression test and it reveals an ultimate strength of 21 MPa and 0.70 ultimate strain.
- Different failure mechanisms were distinguished for sandwich structures under edgewise compression load. With length equal to the width the samples experienced skin-core debonding, shear sliding damage of the skin, and localized buckling in the mid-section of the specimens followed by skin cracking on both sides and progressed throughout the width of the samples. While when length is much greater than the width the global buckling mode is the dominant collapse mode. The ultimate edgewise compressive strength is 85.54 MPa and 14.46 MPa for S-60 and S-200 respectively.

DISCLOSURE STATEMENT

No potential conflict of interest was reported by the authors.

DATA AVAILABILITY STATEMENT

The authors confirm that the data supporting the findings of this study are available within the article.

FUNDING

The author(s) received no financial support for the research, authorship, and/or publication of this article.

REFERENCES

[1] Osa-uwagboe, N., Silberschimdt, V. V., Aremi, A., Demirci, E. (2023). Mechanical behaviour of fabric-reinforced plastic sandwich structures : A state- of-the-art review, J. Sandw. Struct. Mater., 25(5), pp. 591–622, DOI: 10.1177/10996362231170405.

[2] Khechai, A., Tati, A., Guerira, B., Guettala, A., Mohite, P.M. (2018). Strength degradation and stress analysis of composite plates with circular, square and rectangular notches using digital image correlation, Compos. Struct., 185(November 2017), pp. 699–715, DOI: 10.1016/j.compstruct.2017.11.060.

[3] Bouaziz, A., Zaïri, F., Naït-Abdelaziz, M., Gloaguen, J.M., Lefebvre, J.M. (2007). Micromechanical modelling and experimental investigation of random discontinuous glass fiber polymer-matrix composites, Compos. Sci. Technol., 67(15–16), pp. 3278–3285, DOI: 10.1016/j.compscitech.2007.03.031.

[4] Khan, T., Acar, V., Aydin, M.R., Hülagü, B., Akbulut, H., Seydibeyoğlu, M.Ö. (2020). A review on recent advances in sandwich structures based on polyurethane foam cores, Polym. Compos., 41(6), pp. 2355–2400, DOI: 10.1002/pc.25543.

[5] Hopkins, P.M., Norris, T., Chen, A. (2017). Creep behavior of insulated concrete sandwich panels with fiber-reinforced polymer shear connectors, Compos. Struct., 172, pp. 137–146, DOI: 10.1016/j.compstruct.2017.03.038.

[6] Pascual, C., Montali, J., Overend, M. (2017). Adhesively-bonded GFRP-glass sandwich components for structurally efficient glazing applications, Compos. Struct., 160, pp. 560–573, DOI: 10.1016/j.compstruct.2016.10.059.

[7] Kulpa, M., Siwowski, T. (2019). Stiffness and strength evaluation of a novel FRP sandwich panel for bridge redecking, Compos. Part B Eng., 167(November 2018), pp. 207–220, DOI: 10.1016/j.compositesb.2018.12.004.

[8] Mohamed, M., Anandan, S., Huo, Z., Birman, V., Volz, J., Chandrashekhara, K. (2015). Manufacturing and characterization of polyurethane based sandwich composite structures, Compos. Struct., 123, pp. 169–179, DOI: 10.1016/j.compstruct.2014.12.042.

[9] Tuwair, H., Hopkins, M., Volz, J., ElGawady, M.A., Mohamed, M., Chandrashekhara, K., Birman, V. (2015). Evaluation of sandwich panels with various polyurethane foam-cores and ribs, Compos. Part B Eng., 79, pp. 262–276, DOI: 10.1016/j.compositesb.2015.04.023.

[10] Xie, H., Wan, L., Wang, B., Pei, H., Liu, W., Yue, K., Wang, L. (2020). An Investigation on Mechanical Behavior of Tooth-Plate-Glass-Fiber Hybrid Sandwich Beams, Adv. Polym. Technol., 2020,.

[11] Cui, Y., Hao, H., Li, J., Chen, W. (2021). Failure mechanism of geopolymer composite lightweight sandwich panel under flexural and edgewise compressive loads, Constr. Build. Mater., 270, pp. 121496, DOI: 10.1016/j.conbuildmat.2020.121496.

[12] Atiki, E., Khechai, A., Taallah, B., Feia, S., Almeasar, K.S., Guettala, A., Canpolat, O. (2023). Assessment of flexural behavior of compressed earth blocks using digital image correlation technique: effect of different types of date palm fibers, Eur. J. Environ. Civ. Eng., 0(0), pp. 1–22, DOI: 10.1080/19648189.2023.2245868.

[13] Tekieli, M., De Santis, S., de Felice, G., Kwiecień, A., Roscini, F. (2017). Application of Digital Image Correlation to composite reinforcements testing, Compos. Struct., 160, pp. 670–688, DOI: 10.1016/j.compstruct.2016.10.096.

[14] Chakraborty, S., Reddy, S., Subramaniam, K.V.L. (2021). Experimental evaluation and analysis of flexural response of sandwich beam panels with an expanded polystyrene core, Structures, 33(April 2020), pp. 3798–3809, DOI: 10.1016/j.istruc.2021.06.088.

[15] Hosseini-Toudeshky, H., Navaei, A. (2023). Characterization of elastic modulus at glass/fiber interphase using single

fiber composite tensile tests and utilizing DIC and FEM, Mech. Adv. Mater. Struct., 0(0), pp. 1–13, DOI: 10.1080/15376494.2023.2225056.
[16] (2014).ASTM D638-14 Standard Test Method for Tensile Properties of Plastics.
[17] (1996).ISO 1172, Plastiques renforcés de verre textile — Préimprégnés, compositions de moulage et stratifiés — Détermination des taux de verre textile et de charge minérale par des méthodes calcination.
[18] (2015).ASTM D695−15 Standard Test Method for Compressive Properties of Rigid Plastics.
[19] Instron. (2014). A Review of Current In-Plane Composites Compression Testing Methods & Standards, .
[20] (2003).ASTM C 365-00, Standard Test Method for Flatwise Compressive Properties of Sandwich Cores 1.
[21] (2012).ASTM C364/364M-07 Standard Test Method for Edgewise Compressive Strength of Sandwich.
[22] Casavola, C., Del Core, L., Moramarco, V., Pappalettera, G., Patronelli, M. (2022). Full-field mechanical characterization of polyurethane foams under large deformations by digital image correlation, Mech. Adv. Mater. Struct., 29(24), pp. 3540–3555, DOI: 10.1080/15376494.2021.1905915.
[23] Blaber, J., Adair, B., Antoniou, A. (2015). Ncorr: Open-Source 2D Digital Image Correlation Matlab Software, Exp. Mech., 55(6), pp. 1105–1122, DOI: 10.1007/s11340-015-0009-1.
[24] Zeroual, A., Bouaziz, A., Dadda, A., Feia, S., Khechai, A., Lamouri, B., El Hajjar, A. (2023). Experimental investigation on the desiccation cracking process in date palm fiber reinforced clayey soil using digital image correlation, Eur. J. Environ. Civ. Eng., 0(0), pp. 1–22, DOI: 10.1080/19648189.2023.2244555.
[25] Kim, D. (Dae-W., Hennigan, D.J., Beavers, K.D. (2010). Effect of fabrication processes on mechanical properties of glass fiber reinforced polymer composites for 49 meter (160 foot) recreational yachts, Int. J. Nav. Archit. Ocean Eng., 2(1), pp. 45–56, DOI: 10.2478/ijnaoe-2013-0019.